J. Fluid Mech. (2010), *vol.* 659, *pp.* 94–115.
doi:10.1017/S0022112010002363

On the roles of chord-wise flexibility in a flapping wing with hovering kinematics

JEFF D. ELDREDGE†, JONATHAN TOOMEY AND ALBERT MEDINA

Mechanical & Aerospace Engineering Department, University of California, Los Angeles, Los Angeles, CA 90095-1597, USA

(Received 8 July 2009; revised 16 April 2010; accepted 16 April 2010; first published online 24 June 2010)

The aerodynamic performance of a flapping two-dimensional wing section with simplified chord-wise flexibility is studied computationally. Bending stiffness is modelled by a torsion spring connecting two or three rigid components. The leading portion of the wing is prescribed with kinematics that are characteristic of biological hovering, and the aft portion responds passively. Coupled simulations of the Navier–Stokes equations and the wing dynamics are conducted for a wide variety of spring stiffnesses and kinematic parameters. Performance is assessed by comparison of the mean lift, power consumption and lift per unit power, with those from an equivalent rigid wing, and two cases are explored in greater detail through force histories and vorticity snapshots. From the parametric survey, four notable mechanisms are identified through which flexible wings behave differently from rigid counterparts. Rigid wings consistently require more power than their flexible counterparts to generate the same kinematics, as passive deflection leads to smaller drag and torque penalties. Aerodynamic performance is degraded in very flexible wings undergoing large heaving excursions, caused by a premature detachment of the leading-edge vortex. However, a mildly flexible wing has consistently good performance over a wide range of phase differences between pitching and heaving – in contrast to the relative sensitivity of a rigid wing to this parameter – due to better accommodation of the shed leading-edge vortex into the wake during the return stroke, and less tendency to interact with previously shed trailing-edge vortices. Furthermore, a flexible wing permits lift generation even when the leading portion remains nearly vertical, as the wing passively deflects to create an effectively smaller angle of attack, similar to the passive pitching mechanism recently identified for rigid wings. It is found that an effective pitch angle can be defined that accounts for wing deflection to align the results with those of the equivalent rigid wing.

Key words: flow–structure interactions, swimming/flying, vortex shedding

1. Introduction

Biological mechanisms for flight offer intriguing possibilities for novel designs of micro air vehicles. In particular, many airborne insects exhibit a robust hovering capability by flapping their wings in a generally horizontal stroke plane (Ellington 1984). Such observed performance has recently spawned a number of investigations

† Email address for correspondence: eldredge@seas.ucla.edu

of the aerodynamics of flapping in a hovering mode (see e.g. Wang 2005). Insect wings, though highly variable between species, are intricate flexible structures that lack active control features (Dudley 2000). It is therefore impossible to discharge the aerodynamic role of the large passive deformations exhibited by many insects in flight. What is still unclear is whether such deformation provides aerodynamic benefit.

The coupled fluid–structure problem of a flapping-wing flight poses difficulty for any mode of analysis, so investigators of biologically inspired flight have only recently turned their attention away from idealized rigid wings. Some hope for making the problem more tractable can be found in the work of Combes & Daniel (2003), who determined that the inertial and elastic forces generated in a flapping insect wing are significantly larger than the estimated aerodynamic forces. This suggests that it may be possible to decouple the problem, that is, conduct computational aerodynamic studies with prescribed wing deformation, determined from an *a priori* structural computation. The present investigation focuses entirely on fully coupled simulations, leaving further testing of this intriguing hypothesis for future studies.

In an attempt to distil the flexible flapping problem into a simpler version, Toomey & Eldredge (2008) conducted a computational and experimental study of an articulated two-dimensional wing section consisting of two rigid components connected by a linear torsion spring. The model is useful because it reduces the structural complexity while preserving the essential characteristics of chordwise flexibility. For many insects, a significant portion of the wing deformation occurs in the proximity of a dominant spanwise flexion line near the median axis (Dudley 2000). Though a two-dimensional problem clearly lacks many critical features of the full three-dimensional flapping wing, such as spanwise flow and tip effects (Maxworthy 1979; van den Berg & Ellington 1997), the problem nonetheless serves as an important entry in a sequence of canonical problems of increasing complexity. The cataloguing of important phenomena in this simpler problem will facilitate a focused investigation of more sophisticated examples, including three-dimensional flapping.

Much of the focus of the study by Toomey & Eldredge (2008) was on assessing the influence of transition speeds in wing kinematics on wing deflection and generated lift. (Note that the term 'wing' used in this paper generally refers to a planar section.) The flapping kinematics were varied from smooth sinusoidal motions to more rapid transitions in both wing rotation (pitching) and translation (heaving). Comparisons of wing deflection angle and vortex trajectories in the wake between experiments and computations demonstrated very good agreement. It was found that high rotation rates led to large transient responses in lift and wing deflection, in contrast to the steadier lift and smaller deflections produced by sinusoidal motions. The Reynolds number had little effect on the wing deformation, but had a notable impact on the mean lift.

A study recently conducted by Vanella *et al.* (2009) focused on a wing with the same two-component structure as that of Toomey & Eldredge (2008), though with a smooth aerodynamic surface enclosing the structure and a body–fluid mass ratio five times larger. This investigation focused primarily on the effect of spring stiffness and Reynolds number. The authors found that aerodynamic performance (measured by the ratio of mean lift to mean drag and by the lift per unit power) was enhanced for certain stiffnesses. They interpreted their optimal stiffness in terms of the ratio of driving frequency to the natural structural frequency, and noted that this ratio (1/3) coincided with a nonlinear resonance of the structure (perceived as a double pendulum).

For large mass ratios such as the ratio of 25 considered by Vanella *et al.* (2009), the natural frequency of the system is expected to depend primarily on the structural properties. However, at the lower mass ratio of 5 considered in the present paper, the

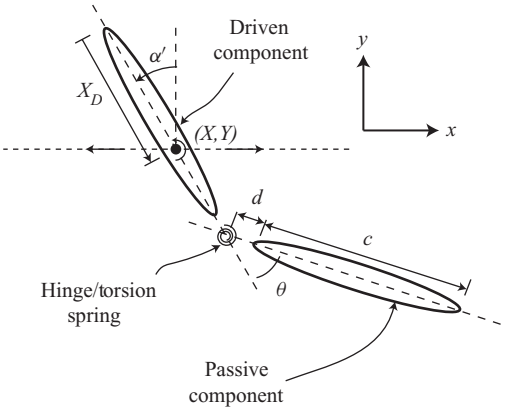

FIGURE 1. The model system consisting of two rigid elliptical sections connected by a hinge with torsion spring.

added fluid inertia and vortex dynamics will significantly affect the natural system response, making resonance more difficult to identify. Many studies – including the present one – have shown that aerodynamic performance depends crucially on the subtle timing of vortex shedding and the subsequent wing–vortex interactions (Wang 2000; Vanella *et al.* 2009). Unfortunately, these complex nonlinear interactions are difficult to account for in low-order aeroelastic models of the system. (An interesting exception to this is in the recent work by Michelin, Llewelyn Smith & Glover (2008), who analysed the behaviour of a flapping flag with an elegant point-vortex model.) Though such low-order models are ultimately necessary as components of flight-control strategies for artificial flapping-wing fliers, it is still necessary to rely on parametric studies with high-fidelity numerical simulation to isolate critical phenomena.

This study utilizes the same two-component wing problem as investigated by Toomey & Eldredge (2008) and Vanella *et al.* (2009), and also makes use of an analogous three-component wing. The objective of this study is to identify the principal mechanisms by which aerodynamic performance is notably affected by wing flexibility. These mechanisms are identified through variation of four key kinematic parameters that have thus far been omitted from the previous explorations: heaving amplitude, chordwise position of the rotation axis, the phase difference between pitching and heaving, and pitching amplitude. It will be shown that these parameters play a critical role in determining aerodynamic performance. Two notable examples will be highlighted to illustrate cases in which aerodynamic performance is deteriorated or improved from a corresponding rigid wing. The problem statement is described in § 2 and the methodology is briefly described in § 3. The results of the study are presented in § 4, and the detailed analysis of the two cases is described in § 5.

2. Problem statement

This investigation focuses on the same two-dimensional model that was investigated by Toomey & Eldredge (2008) (and nearly the same as that investigated by Vanella *et al.* 2009): a wing composed of two rigid components connected by a hinge with torsion spring (figure 1). The kinematics of a pitching axis through the lead body – at a distance X_D from the leading edge – are prescribed, while the trailing body is allowed to respond passively. The angular deflection of this passive component from

equilibrium is measured by θ. Both constituent bodies are 5:1 elliptic cross-sections, with major axis length c. The gap between the bodies is transparent to the flow to simplify the numerics; the distance from the nearest edge of each ellipse to the hinge is $d = 0.05c$, and the total length of the body is $L = 2.1c$. The gap has little effect on the aerodynamics, as demonstrated by comparison with a monolithic wing of the same length and thickness (Toomey 2009). The density of the trailing body, ρ_b, is five times the density of the surrounding fluid, ρ_f. The linear torsion spring has dimensional stiffness K^* and damping coefficient R^*.

The investigation also makes use of an analogous three-component model, consisting of three equal 6.125:1 ellipses with gap half-width $d = 0.03125c$ and a total length $L = 3.125c$, where c is the length of each constituent body. The densities of these bodies are also five times the density of the fluid.

2.1. *Kinematics and dimensionless parameters*

A parametrized family of kinematics is used to prescribe oscillatory rectilinear translational ('heaving') and rotational ('pitching') motion of the pitching axis through the lead body. These kinematics are described mathematically as

$$X(t) = \frac{A_0}{2}\frac{G_t(ft)}{\max G_t}C(ft), \tag{2.1}$$

$$\alpha'(t) = -\alpha'_0\frac{G_r(ft)}{\max G_r} \tag{2.2}$$

(and $Y = 0$) where f is the frequency, and the translational shape function is

$$G_t(t) = \int_0^t \tanh\left(\sigma_t \cos\left(2\pi t'\right)\right) \mathrm{d}t'. \tag{2.3}$$

The rotational shape function is

$$G_r(t) = \tanh\left(\sigma_r \cos\left(2\pi t + \Phi\right)\right). \tag{2.4}$$

The translation kinematics have been modified with a start-up conditioner

$$C(t) = \frac{\tanh\left(8t - 2\right) + \tanh 2}{1 + \tanh 2} \tag{2.5}$$

to avoid impulsive velocity changes. This conditioner primarily affects only the first period of motion. The phase Φ controls the lead of the pitching relative to the heaving; at a value of $\Phi = 0$, the wing is undergoing its peak angular velocity at the instant of heave reversal. This kinematic model was also used in the previous investigation of Toomey & Eldredge (2008), which focused on the influence of the non-dimensional translational and rotational shape coefficients, σ_t and σ_r. In the studies reported in the present paper, unless otherwise stated, these coefficients are both held fixed at $\pi/5$, which provides nearly sinusoidal pitching and heaving. The dimensionless kinematic parameters investigated in the present studies are the heaving amplitude A_0/L, the pitching phase lead Φ, the position of the pitching axis X_D/L and the pitching amplitude α'_0. In the studies in which pitching amplitude α'_0 is not varied, it is fixed at 45°. Figure 2 depicts a diagram that illustrates these kinematics for two different choices of phase lead.

The kinematic parameters lead to the following definition of the translational Reynolds number, based on the peak translational velocity V:

$$Re_t = \frac{VL}{\nu}. \tag{2.6}$$

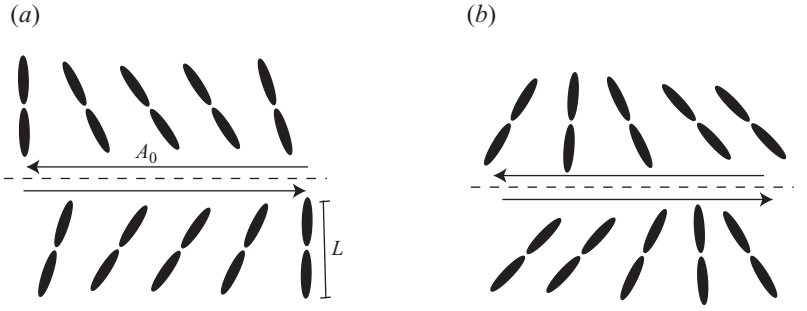

FIGURE 2. Sample flapping kinematics with $A_0/L = 2.67$, $X_D/L = 0.48$. Pitching phase lead $\Phi = 0$ (*a*) and $\Phi = 45^\circ$ (*b*).

(Note that this definition is somewhat different from that of Toomey & Eldredge 2008.) Throughout these studies the translational Reynolds number is fixed at 220. The normalized spring damping coefficient of the two-component wing, $R = R^*/(\rho_f f L^4)$, is held fixed at the value 0.2 for all studies in this paper. The normalized stiffness of the torsion spring, $K = K^*/(\rho_f f^2 L^4)$, varies between the values 5.1, 23.5 and 51.4. (The first and third have the values 100 and 1000 when normalized by c instead of L, and the second is the value corresponding to the experiments of Toomey & Eldredge 2008.) Results from wings with these stiffnesses are compared with an equivalent wing with hinge rigidly locked at zero deflection angle. For the studies with a three-component wing, the two hinges have damping coefficients of $R_1 = 0.6785$ and $R_2 = 0.4830$, and stiffnesses $K_1 = 228$ and $K_2 = 163$, respectively.

2.2. *Performance metrics*

The aerodynamic response of the flapping wing is characterized by three performance metrics: the mean lift $\bar{F}_y$, the mean power input to the system $\bar{P}$ and the mean lift per unit power $\bar{F}_y/\bar{P}$. The last metric is meant to characterize the efficiency of the flapping wing: larger values represent more efficient access to a desired amount of lift. These quantities are normalized by length scale L and by two different time scales: by a frequency scaling (e.g. $2\bar{F}_y/(\rho_f f^2 L^3)$) or by the maximum translational velocity V (e.g. $2\bar{F}_y/(\rho_f V^2 L)$, $2\bar{P}/(\rho_f V^3 L)$ and $\bar{F}_y V/\bar{P}$).

3. Methodology

The simulations of this investigation are carried out with the viscous vortex particle method (Eldredge 2007, 2008), which solves the Navier–Stokes equations with strong dynamical coupling to the equation for the angular deflection θ of the passive trailing body, e.g. for two components,

$$\left(I + mL_2^2\right)\ddot{\theta} + R^*\dot{\theta} + K^*\theta = -mL_2\cos(\alpha' + \theta)\ddot{X} - \left[I + m\left(L_2^2 + L_1L_2\cos\theta\right)\right]\ddot{\alpha}' - (mL_1L_2\sin\theta)\,\dot{\alpha}'^2 + M_h, \quad (3.1)$$

where m and I are the mass and second moment of inertia (per unit depth) of the passive component body, respectively; $L_1 = d + c - X_D$ is the distance from the pitching axis to the hinge; $L_2 = d + c/2$ is the distance from the hinge to the centroid of the passive body and M_h is the fluid dynamic moment exerted on the passive body about the hinge axis. A similar equation can be derived for more than two components (Eldredge 2008).

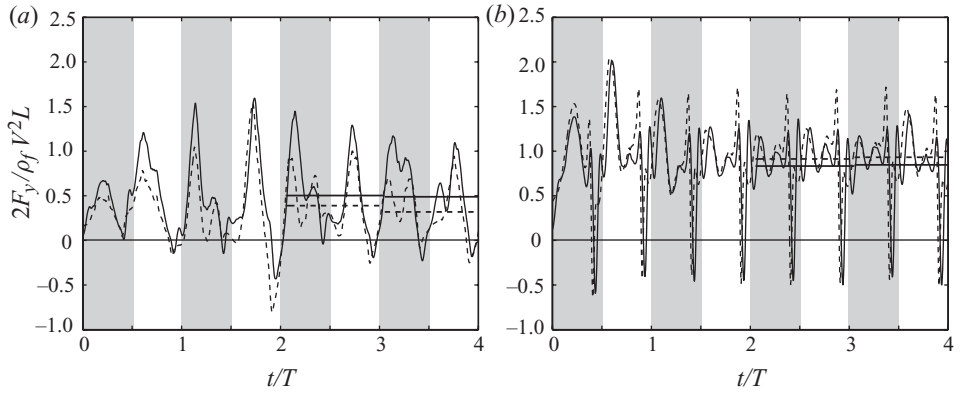

FIGURE 3. Lift histories at $A_0/L = 4$ for $\alpha_0' = 10°$ (*a*) and $\alpha_0' = 40°$ (*b*). Flexible three-component wing (—); rigid one-component wing (– –). The pitching phase lead is 36° and pitch axis is $X_D/L = 0.16$. The alternate shaded and unshaded intervals correspond to heaving half-strokes, and mean values over given intervals are depicted.

The details of the methodology have been presented – and its convergence demonstrated – in previous papers (Eldredge 2007, 2008), to which the interested reader is referred. The accuracy of the method for the present flapping-wing configuration was shown by Toomey & Eldredge (2008) through comparison with experimental results.

The simulations conducted in this investigation are carried out for three cycles of flapping, and the average is computed from two overlapping period-long intervals: the third flapping cycle $[2T, 3T]$ and the cycle one quarter period earlier $[1.75T, 2.75T]$. It is noted that three cycles are not always sufficient to achieve a stationary periodic state in the aerodynamics. Many cases resemble those shown in figure 3, which compares the lift generated by the three-component and one-component wings at two different pitch amplitudes. Except for some differences in the one-component wing at $\alpha_0' = 10°$, the lift signature of the fourth stroke is generally similar to that of the third stroke, and the mean value changes only slightly (at most by 18 %). Sequential half-strokes exhibit less similarity with each other, due to a lingering memory of the initial half-stroke. However, a few unusual cases exhibit more significant variation from the third to the fourth stroke. For example, figure 4 depicts four cycles of the lift generated by the two-component wing with rigidly locked hinge, for heaving amplitude $A_0/L = 2.67$, pitching phase lead $\Phi = 67.5°$ and pitch axis $X_D/L = 0.48$. In this case, the lift signature changes dramatically, and the mean lift increases from 0.17 to 0.41. As the analysis of § 5 will demonstrate, such cases that exhibit little repeatability after four strokes are characterized by shed vorticity that interacts multiple times with the wing. This variable behaviour is generally established by the third stroke, and occurs only in two cases reported in this study. In both of these, the pitching leads the heaving, and the cases are noted in the text.

4. Results

In this section, the results of the parametric computational studies are reported. The heave amplitude A_0/L, pitching axis location X_D/L and pitching phase lead Φ of the two-component wing are all varied in turn, and the results are obtained for three different hinge stiffnesses and compared with the corresponding rigid wing.

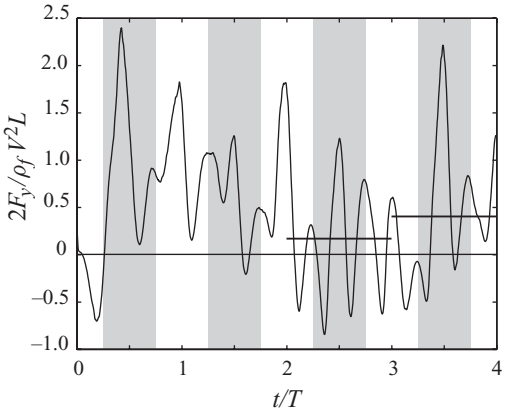

FIGURE 4. Lift history for a rigid two-component wing at heave amplitude $A_0/L = 2.67$, pitching phase lead $\Phi = 67.5^\circ$ and pitch axis $X_D/L = 0.48$.

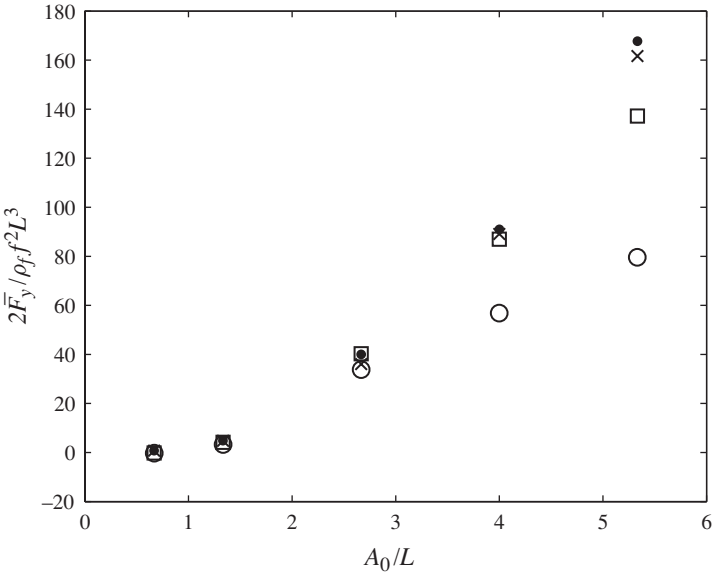

FIGURE 5. Mean lift versus heave amplitude for a phase of $\Phi = 0$ and pitching axis at $X_D/L = 0.48$. ○, $K = 5.1$; □, $K = 23.5$; ×, $K = 51.4$; ●, rigid.

In addition, a study of the effect of the pitching amplitude α_0' is presented for the three-component wing.

4.1. *Performance with varying heave amplitude*

In this set of cases, the wing pitches about an axis located at $X_D/L = 0.48$, just forward of the hinge. The pitching phase lead is fixed at $\Phi = 0$ – that is, the wing changes heave direction at the same instant at which it achieves its maximum pitching rate. The heave amplitude A_0/L is varied from 0.67 to 5.33.

The resulting mean lift scaled by frequency is depicted in figure 5. For the rigid wing and all flexible ones, the lift increases monotonically with increasing heave amplitude. The maximum heave velocity, V, increases linearly with heave amplitude, so the plot demonstrates the expected increase of lift with increasing heave velocity.

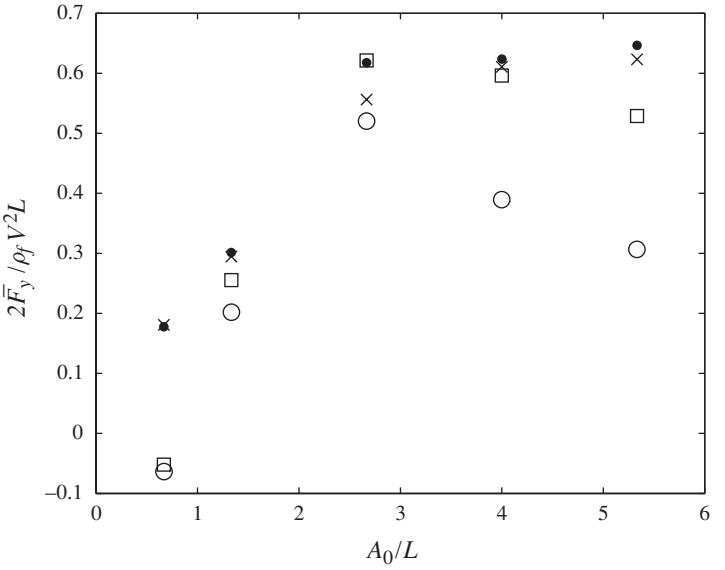

FIGURE 6. Mean lift, rescaled with maximum heave velocity of the pitching axis V, versus heave amplitude for various stiffnesses. ○, $K = 5.1$; □, $K = 23.5$; ×, $K = 51.4$; ●, rigid. Phase $\Phi = 0$ and driving axis at $X_D/L = 0.48$.

At low heave amplitudes, the lift values from all wings are nearly indistinguishable, though in fact the two most flexible wings produce slightly negative mean lift. At high heave amplitudes, the stiffest wing, $K = 51.4$, generates nearly the same lift as the rigid wing, while the $K = 23.5$ wing generates slightly less lift, and the most flexible wing, $K = 5.1$, produces significantly less lift.

The trend of the mean lift in figure 5 is expected, because no information about the changing heave velocity is encoded in the scaling for the lift. In figure 6, the lift is plotted again, but now scaled with $\rho_f V^2 L/2$. This scaling is not as physically relevant at low heave amplitudes, at which the lift is primarily generated by wing rotation (Toomey & Eldredge 2008). Consequently, the scaled lift varies considerably over this range of A_0/L. However, the scaling reveals some subtlety in the dependence of lift on higher values of heave amplitude. Above $A_0/L = 2.67$, the lift of the rigid and stiffest flexible wings reaches a nearly constant value, while the lift generated by the two most flexible wings tends to drop with increasing A_0/L. This behaviour will be explored in more detail in § 5.1.

Similar trends at large A_0/L are exhibited in the power consumption, depicted in figure 7. It is important to note that the rigid wing consistently requires the most power to enable the flapping kinematics. This observation holds in almost all cases considered in this paper. Drag and torque tend to be the dominant influences that must be overcome in flapping, and these are generally smaller for flexible wings because of the lower profile such wings present to the flow when the wing is deformed. The mean lift per unit power consumed – or flapping efficiency – is shown in figure 8 and rises to a plateau of approximately 0.8 at $A_0/L = 2.67$ for all wings, with slight decay at larger A_0/L for some of the wings.

It is instructive to re-plot the lift and efficiency results for large A_0/L with varying stiffness on the abscissa, in order to more clearly illustrate the dependence on wing flexibility. In figure 9, stiffness variation is represented indirectly by plotting

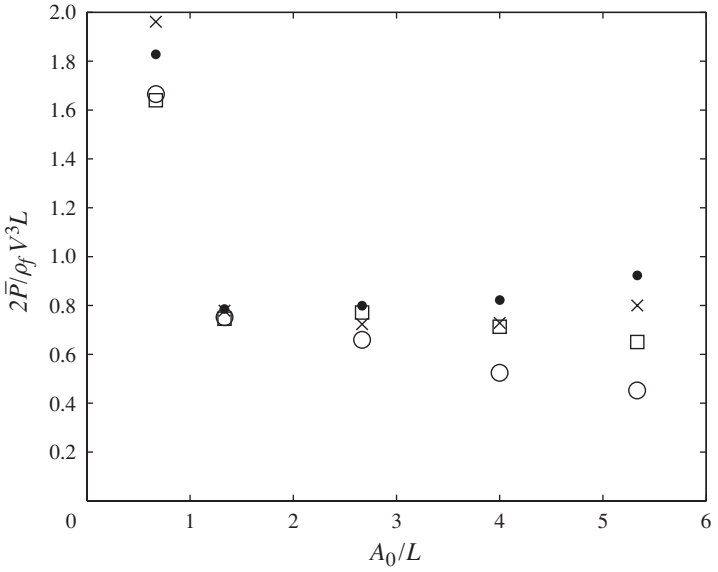

FIGURE 7. Mean power consumed versus heave amplitude for a phase of $\Phi = 0$ and pitching axis at $X_D/L = 0.48$. ○, $K = 5.1$; □, $K = 23.5$; ×, $K = 51.4$; ●, rigid.

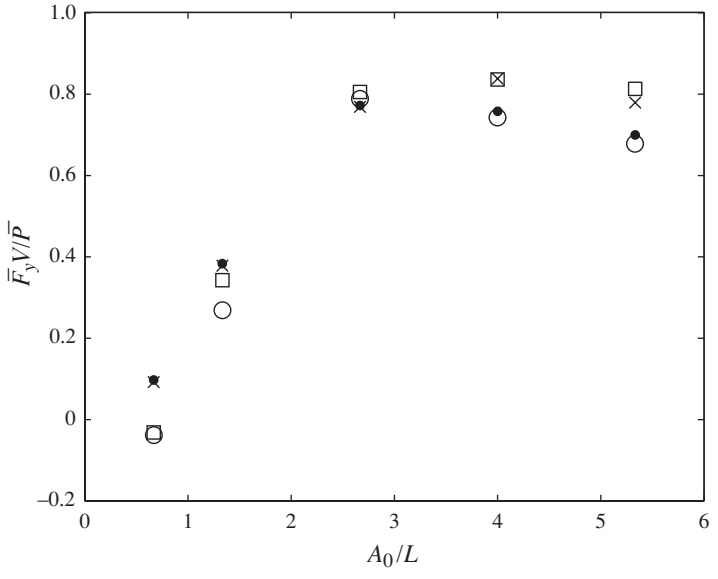

FIGURE 8. Mean lift force per unit power consumed versus heave amplitude for a phase of $\Phi = 0$ and pitching axis at $X_D/L = 0.48$. ○, $K = 5.1$; □, $K = 23.5$; ×, $K = 51.4$; ●, rigid.

versus $K^{-1/2}$, which is a dimensionless frequency in which the scaling parameter, $(K^*/\rho_f L^4)^{1/2}$, is proportional to the fundamental frequency of the system. However, the constant of proportionality depends not only on the wing structure but also on the added inertia imparted by the fluid as well as the vortex dynamics, and is difficult to predict *a priori*. Figure 9, which includes an extra set of runs conducted at a fourth stiffness ($K = 9.8$), demonstrates that the rigid wing (zero scaled frequency) generates the largest lift at all three heave amplitudes, and lift decreases more rapidly with scaled

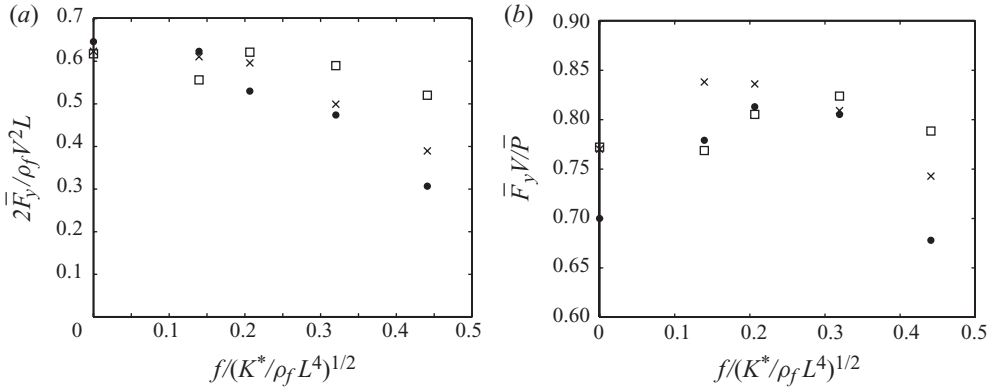

FIGURE 9. Mean lift force (*a*) and mean lift per unit power consumed (*b*) versus normalized frequency for phase $\Phi = 0$ and pitching axis at $X_D/L = 0.48$. □, $A_0/L = 2.67$; ×, $A_0/L = 4$; ●, $A_0/L = 5.33$.

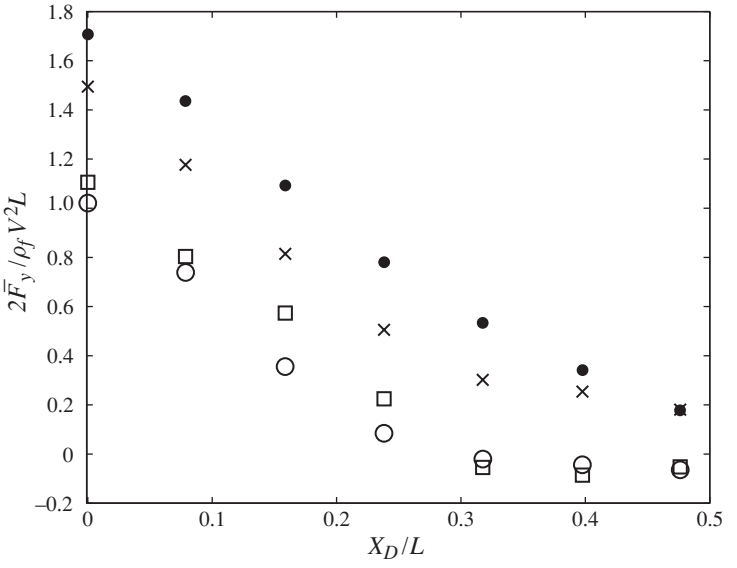

FIGURE 10. Mean lift versus pitching axis position for a heave amplitude $A_0/L = 0.67$ and pitching phase lead $\Phi = 0$. ○, $K = 5.1$; □, $K = 23.5$; ×, $K = 51.4$; ●, rigid.

frequency as heave amplitude increases. Efficiency, however, reaches a maximum value at a frequency that depends on the heave amplitude. This relationship between optimal frequency and heave amplitude is apparently not monotonic: for $A_0/L = 2.67$, the peak efficiency occurs at $K^{-1/2} \approx 0.31$, at $A_0/L = 4$ it occurs at $K^{-1/2} \approx 0.14$ and at $A_0/L = 5.33$, the peak is approximately centred at $K^{-1/2} = 0.2$. Furthermore, the peak efficiency is largest when $A_0/L = 4$.

4.2. *Performance with varying position of pitching axis*

Figures 10–12 depict the lift, power consumption and flapping efficiency, respectively, as the position of the driving axis is moved from the leading edge towards the hinge axis. The other kinematic parameters are held constant: $A_0/L = 0.67$, $\Phi = 0$ and $\alpha_0' = 45°$. The heave amplitude is relatively small in this set of cases. From the previous

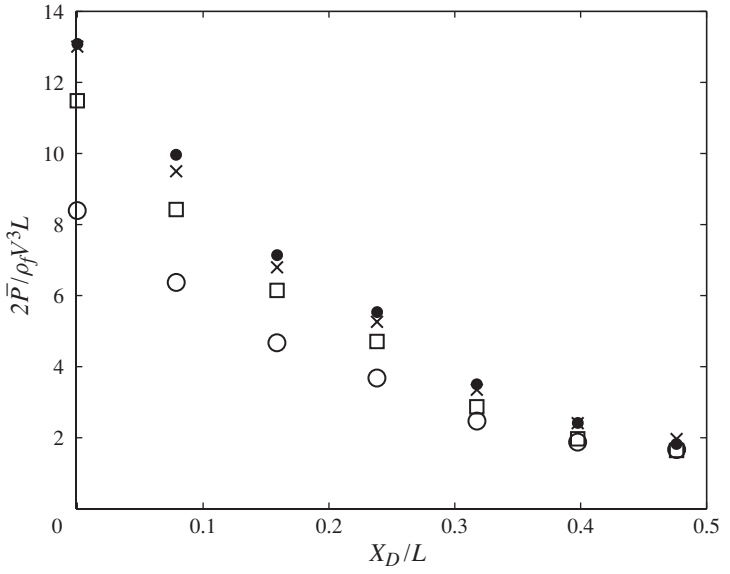

FIGURE 11. Mean power consumed versus pitching axis position for a heave amplitude $A_0/L = 0.67$ and pitching phase lead $\Phi = 0$. ○, $K = 5.1$; □, $K = 23.5$; ×, $K = 51.4$; ●, rigid.

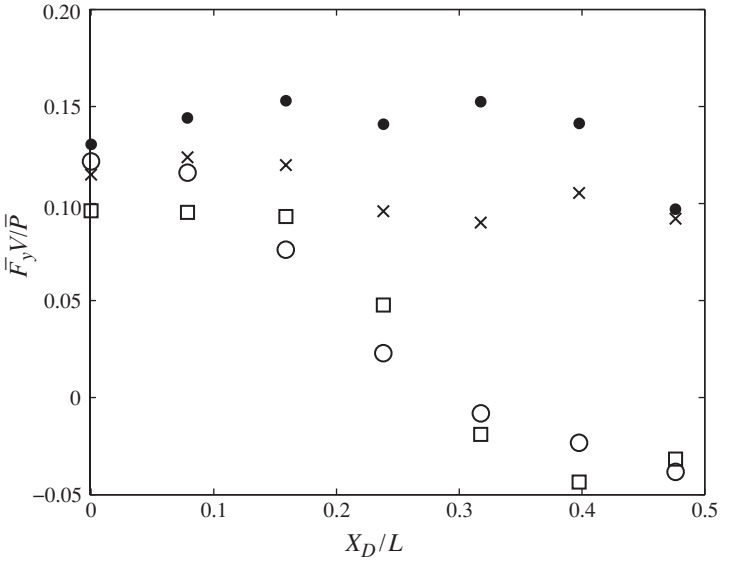

FIGURE 12. Mean lift per unit power consumed versus pitching axis position for a heave amplitude $A_0/L = 0.67$ and pitching phase lead $\Phi = 0$. ○, $K = 5.1$; □, $K = 23.5$; ×, $K = 51.4$; ●, rigid.

section, it was found that the perfectly rigid and stiffest wings generate the most lift and achieve the highest efficiency – nearly identically – at this amplitude when phase lead is zero and pitching axis is at $X_D/L = 0.48$. In figure 10, it is clear that the rigid wing consistently outperforms all other wings in generating lift at all other pitching axis positions. The lifts of the rigid and stiffest wings decay monotonically

as the pitching axis is moved aft, which is consistent with the results of Dickinson, Lehmann & Sane (1999). In the two most flexible wings, however, the mean lift reaches a minimum at $X_D/L \approx 0.4$, and is negative in a range surrounding this minimum. The moderately flexible wing, $K = 23.5$, has the lowest minimum value, though it generates more lift than the most flexible wing at small values of X_D/L. Figure 11 demonstrates a steady decline in power consumption as the pitch axis is moved towards the centroid of the wing, consistent with the decreased torque required to pitch the wing. This power decreases monotonically with decreasing stiffness, for the reasons described in § 4.1.

The flapping efficiency, displayed in figure 12, demonstrates interesting trends. When the pitching axis is close to the leading edge, all wings perform with nearly the same (low) efficiency. However, the performance of the two most flexible wings drops off quickly as the pitching axis is moved aft of $0.15L$. The rigid and stiffest flexible wings, in contrast, have consistent efficiency at all pitching axis positions.

It is important to note that the results obtained by a change of pitching axis location are not independent of changes in the other kinematic parameters: A_0/L, Φ and α_0'. It is not difficult to show that there is some equivalence between varying the position of the pitching axis and varying these other parameters. For sinusoidal kinematics in both the pitching and heaving with a pitch amplitude $\alpha_0' < 1$, the kinematics imposed on the pitching axis at any location X_D can be written approximately as kinematics imposed about a reference axis (the leading edge, for simplicity):

$$X_0(t) = \frac{A_{0,eff}}{2} \sin(2\pi f t + \Phi_{0,eff}), \tag{4.1}$$

$$\alpha'(t) = -\alpha_0' \cos(2\pi f t + \Phi), \tag{4.2}$$

where

$$A_{0,eff} \approx \left[\left(A_0 - 2X_D \alpha_0' \sin \Phi \right)^2 + 4X_D^2 (\alpha_0')^2 \cos^2 \Phi \right]^{1/2}, \tag{4.3}$$

$$\Phi_{0,eff} \approx \arctan\left(\tan \Phi - \frac{A_0}{2X_D \alpha_0' \cos \Phi} \right) + \frac{\pi}{2}. \tag{4.4}$$

That is, the four-dimensional parametric space given by $(A_0/L, \Phi, \alpha_0', X_D/L)$ is approximately equivalent to a reduced three-dimensional space $(A_{0,eff}/L, \Phi - \Phi_{0,eff}, \alpha_0', 0)$, albeit with some difference in the initial configuration of the wing. Simulations that begin at different points of the flapping cycle lead to differences in the lift histories because of persistent effects on the vortex shedding and pairing. However, the mean values of lift and power are not significantly affected by the initial configuration.

Equations (4.1)–(4.4) show, in particular, that, as the pitching axis is moved aft, the effective phase of heaving is increased, and thus the effective phase lead of pitching to heaving is decreased. This effect is more dramatic for smaller heave amplitudes.

4.3. *Performance with varying phase between pitching and heaving*

In this set of cases, the heave amplitude is fixed at $A_0/L = 2.67$ and the pitching axis at $X_D/L = 0.48$, while the phase lead of pitching is varied from 0 to 67.5. Figures 13–15 display the resulting mean lift, mean power consumption and flapping efficiency, respectively. The values of these quantities at $\Phi = 0$ were depicted in the plots of § 4.1. The moderately flexible wing ($K = 23.5$) generates the largest lift – marginally larger than the rigid wing – under these conditions. When phase lead is increased further, the flexible wings exhibit more consistent lift generation compared to the equivalent rigid wing for the entire range of Φ depicted. When phase lead is

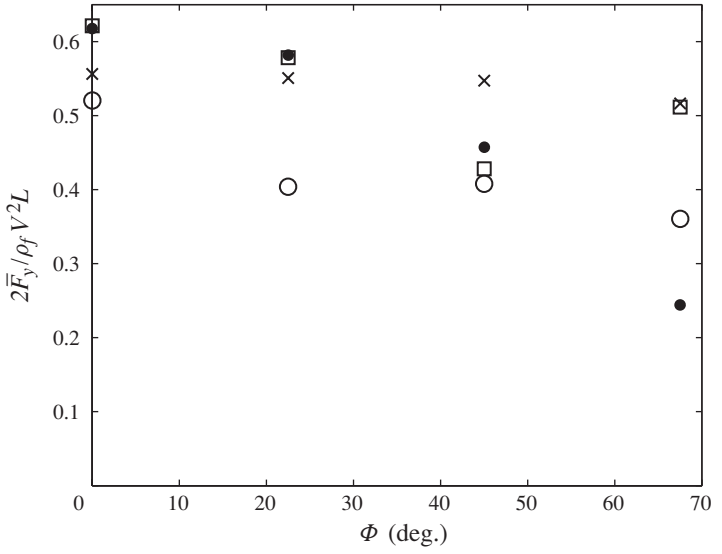

FIGURE 13. Mean lift versus pitching phase lead for a heave amplitude $A_0/L = 2.67$ and driving axis at $X_D/L = 0.48$. ○, $K = 5.1$; □, $K = 23.5$; ×, $K = 51.4$; ●, rigid.

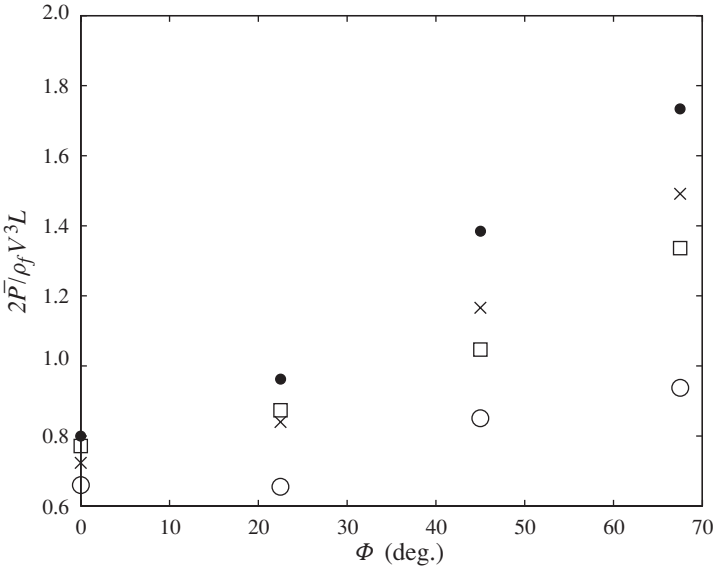

FIGURE 14. Mean power consumed versus pitching phase lead for a heave amplitude $A_0/L = 2.67$ and driving axis at $X_D/L = 0.48$. ○, $K = 5.1$; □, $K = 23.5$; ×, $K = 51.4$; ●, rigid.

increased to $\Phi = 22.5°$, figure 13 shows that the rigid wing generates slightly more lift than the other wings. However, there is a rapid fall in the lift of the rigid wing as phase lead is increased further. The lift from the moderately flexible wing drops significantly at $\Phi = 45°$ (this is the second case referred to in § 3 with significant variation from stroke to stroke due to strong vortex interactions), but recovers at 67.5°. The lift of the most flexible wing is approximately constant, but low, for most phases. However, the lift produced by the stiffest flexible wing is consistently high at all phase leads.

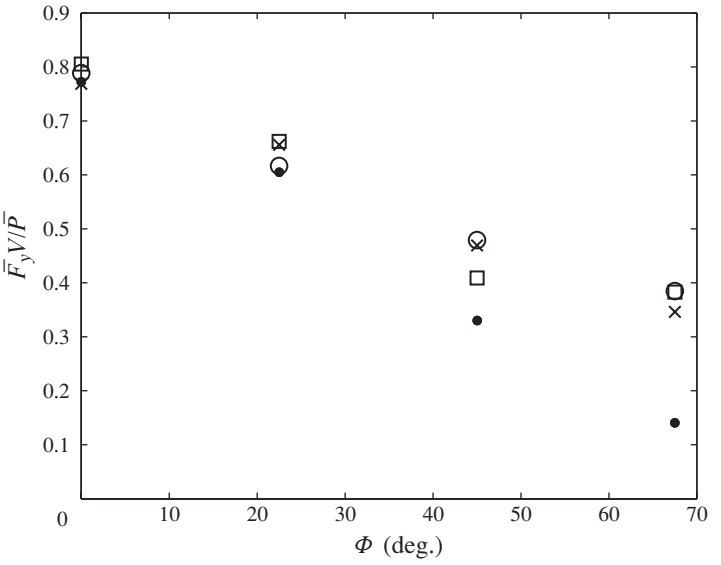

FIGURE 15. Mean lift per unit power consumed versus pitching phase lead for a heave amplitude $A_0/L = 2.67$ and driving axis at $X_D/L = 0.48$. ○, $K = 5.1$; □, $K = 23.5$; ×, $K = 51.4$; ●, rigid.

The power consumed by all wings generally increases as phase lead increases, since a larger drag results from the wider profile presented to the flow during the latter stages of heaving (see figure 2 for example). As in the previous sets of cases, the power consumed by the rigid flapping wing is higher than by all flexible wings. Thus, it is not surprising that the flapping efficiency, depicted in figure 15, is higher for these flexible wings. This efficiency tends to decay as the phase lead increases. It is interesting to note that there is little difference in the magnitudes of these efficiencies between all flexible wings, except for the aforementioned case of $K = 23.5$ at $\Phi = 45°$.

4.4. *Performance with varying pitch amplitude*

The pitch amplitude α_0' controls the degree to which the flapping wing adopts an aerodynamic angle of attack in each direction of heaving. As such, it is expected to control the development of the leading-edge vortex, and the degree to which this vortex contributes positively to lift. A heaving rigid wing with little pitching remains nearly vertical, and in its most extreme case ($\alpha_0' = 0$), will generate negligible lift apart from the small net contribution from the edges if vertical flow symmetry is broken. (If such a wing is free to translate in the direction transverse to the heaving, the broken symmetry will, in some circumstances, lead to net motion in a randomly selected direction; see Vandenberghe, Zhang & Childress 2004.)

Figure 16 depicts the mean lift and flapping efficiency of a three-component (flexible) versus a single-component (rigid) wing undergoing flapping kinematics about a pitch axis at $X_D/L = 0.16$ with phase lead $\Phi = 36°$ and heaving amplitude $A_0/L = 4$. The wing rotation occurs more rapidly ($\sigma_r = 5$) in these cases than in the other studies reported in this paper, ensuring that the pitch angle is nearly constant for most of each half-stroke. Though the rigid wing produces slightly more lift at larger pitch amplitudes, the flexible wing generates larger lift at smaller pitch amplitudes, and in

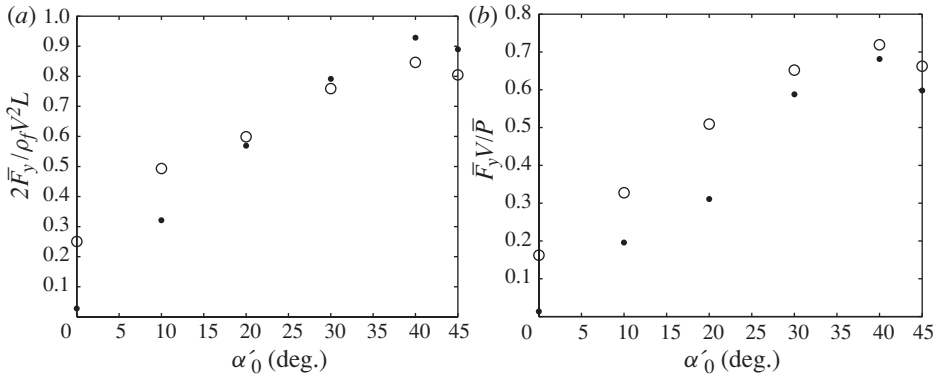

FIGURE 16. Mean lift (*a*) and mean lift per unit power consumed (*b*) versus pitching amplitude for a heave amplitude $A_0/L = 4$ and driving axis at $X_D/L = 0.16$. ○, Flexible 3-component; ●, rigid.

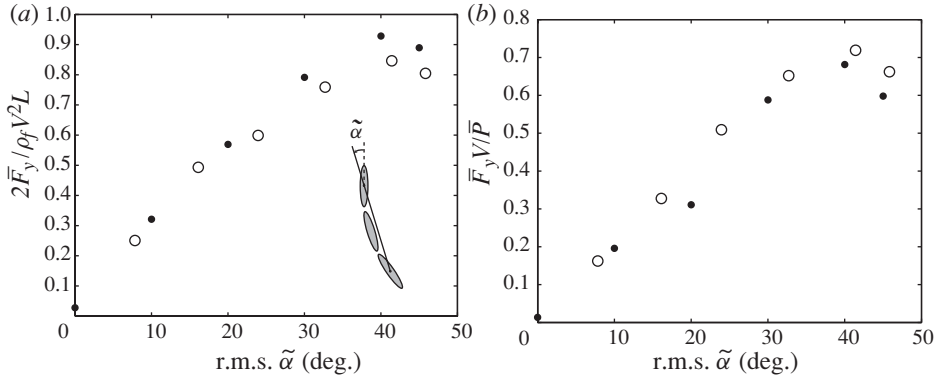

FIGURE 17. Mean lift (*a*) and mean lift per unit power consumed (*b*) versus effective pitching amplitude for a heave amplitude $A_0/L = 4$ and driving axis at $X_D/L = 0.16$. ○, Flexible 3-component; ●, rigid.

particular, non-zero lift at zero pitching. Furthermore, the efficiency of the flexible wing is larger than that of the rigid wing at all pitch amplitudes.

Figure 16 shows that wing flexibility can potentially provide an opportunity for lift generation that is unavailable for a rigid wing flapping at small α'_0. During each heaving phase of the stroke, the flexible portion of the wing deflects opposite the direction of motion, providing the wing with a somewhat smaller effective angle of attack. This passive mechanism for changing the effective angle of attack is very similar to passive pitching of a rigid wing, explored recently by Bergou, Xu & Wang (2007). An effective pitch angle, $\tilde{\alpha}$, can be quantified by measuring the angle of a line intersecting the centroids of the first and last constituent bodies. The lift and efficiency are plotted versus the r.m.s. amplitude of this angle (and of the original pitch angle of the single-component wing) in figure 17. The lift and efficiency trends exhibited by the two wings agree well over the entire range, except for a slightly lower lift and higher efficiency in the flexible wing at the largest angles.

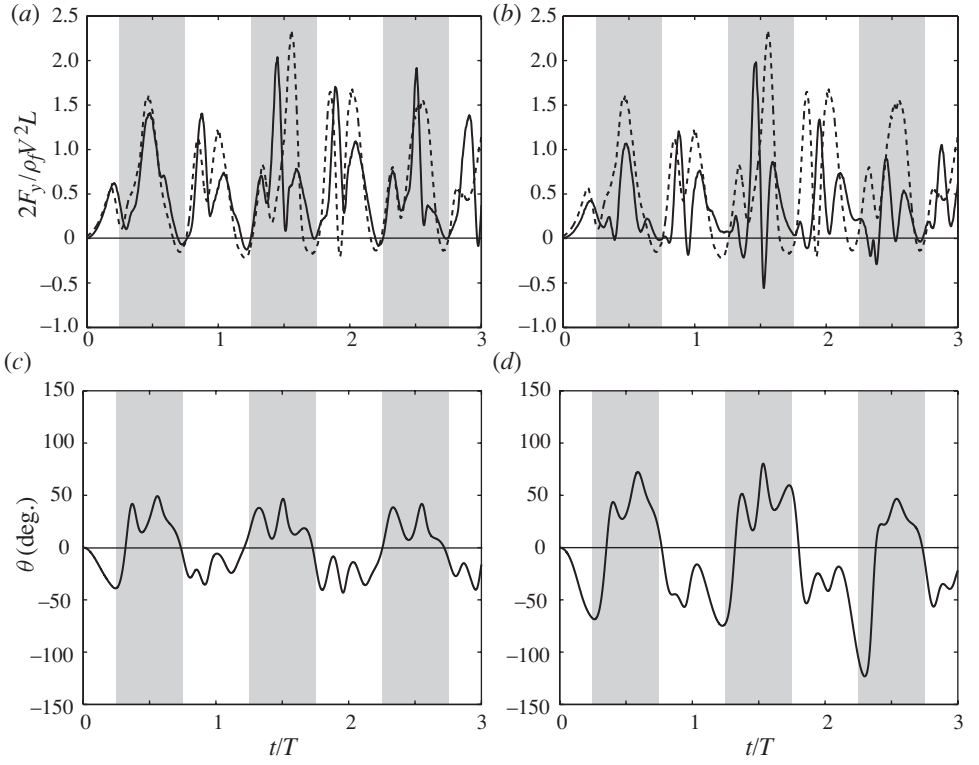

FIGURE 18. Lift (a, b) and hinge deflection (c, d) histories at heave amplitude $A_0/L = 5.33$ for $K = 23.5$ (a, c) and $K = 5.1$ (b, d) torsion springs. The lift on the rigidly linked wing is shown as a dashed line for reference in (a, b). The phase lead of pitching is zero and $X_D/L = 0.48$.

5. Analysis and discussion of two representative cases

From the results depicted in the previous section, there are three primary observations that can be made about flapping with flexible versus rigid wings. Firstly, more flexible wings generate lift relatively poorly at high heave amplitudes. Secondly, the lift generated by flexible wings is relatively insensitive to changes of pitching phase lead, while the lift of the rigid wing falls sharply as phase increases. And finally, flexible wings can generate lift even when the wing undergoes no pitching, whereas the rigid wing cannot. In this section, physical explanations will be offered for the first two trends by examination of the lift histories and vortex shedding patterns of representative cases.

5.1. *Rigid versus flexible wings at high heave amplitude*

Figure 18 depicts the time histories over three cycles of the lift and hinge deflection angle for the two most flexible wings, $K = 23.5$ and $K = 5.1$, at the largest heave amplitude $A_0/L = 5.33$, with $\Phi = 0$ and $X_D/L = 0.48$. It was shown in figure 5 that the lift of these wings under these conditions is significantly smaller than that of the rigid wing. The lift history, which is scaled here by V, is compared with the lift generated by the equivalent rigid wing.

The lift generated by the rigid wing exhibits a characteristic primary peak occurring just after the midpoint of each heaving half-cycle, when the heaving velocity is

largest. A secondary peak precedes this primary peak, though in alternate half-strokes, they are of comparable magnitude. This lift signature is similar to the one observed in the zero-phase simulation and experimental results of Wang, Birch & Dickinson (2004). They ascribed the primary peak to quasi-steady circulatory lift from heaving, which is enhanced by the growth of the leading-edge vortex. The earlier secondary peak was attributed to fundamentally unsteady effects from wing–wake and wake–wake interactions, indicative of the so-called wake-capture mechanism (Dickinson *et al.* 1999). This lift peak occurs just after the wing reversal when heaving acceleration is largest. Thus, it is more likely due to the inertial reaction force of the fluid, slightly delayed while the wing pitches into an angle of attack.

The lift signature generated by the flexible wings differs considerably from that of the rigid wing. During the stroke starting at $t/T = 1.25$, the lift and deflection results shown in figure 18 are similar for the two flexible wings, though the deflection is larger in the more flexible wing. Each half-cycle is characterized by the initial lift peak from inertial reaction of heaving, which is sometimes offset by a downwards inertial reaction as the passive component rapidly rotates backwards during this interval. This is followed by the growth of the primary circulation lift, which then falls precipitously approximately half-way through the heaving (e.g. at $t/T \approx 1.5$, 2, 2.5), and completed by the growth of a final smaller peak. The deflection exhibits multiple oscillations about a mean value during each half-stroke. This mean deflection corresponds to the passive trailing body pushed backwards from its equilibrium position as the wing translates. The results of the flexible wings differ considerably from each other in the half-stroke from $t/T = 2.25$ to 2.75 as the most flexible wing exhibits an anomalously high deflection angle at around $t/T = 2.3$, followed by a primary lift peak with greatly reduced magnitude.

This behaviour can be better understood by examining a few snapshots of the vorticity, as shown in figure 19. These snapshots depict a comparison of the vortex shedding pattern for the most flexible wing and rigid wing at three different instants during the end of one heaving interval. A leading-edge vortex is apparent at $t/T = 2.51$ for both wings, which is indicative of significant lift generation. The trailing body of the flexible wing is significantly deflected, which greatly alters the flow in the vicinity of the trailing edge. At $t/T = 2.61$, this trailing body in the flexible wing is undergoing a clockwise rotation, indicated by the formation of a counterclockwise vortex at its trailing edge. Meanwhile the leading-edge vortex has detached, and a new vortex is under development; the lift has dropped nearly to zero during this interval and is increasing to its small final peak as the new vortex is formed. This flexible wing exhibits oscillations from the coupled elastic deformation and alternating vortex shedding from the leading and trailing edges; during the limited heaving interval the system can only undergo one or two such oscillations.

The leading-edge vortex of the rigid wing, in contrast, has grown larger but is still attached at $t/T = 2.61$; the lift at this instant is nearly at its largest value. It is important to note that a rigid wing would also be expected to undergo alternating vortex shedding (see e.g. Brunton *et al.* 2008), but the heaving interval is not long enough to initiate this behaviour. The elastic structure of the wing evokes the oscillations earlier. In the last row of panels at $t/T = 2.71$, in which both wings are pitching clockwise, the leading- and trailing-edge vortices of the rigid wing differ significantly from those of the flexible wing. The flows into which these wings enter in the following half-stroke are also different, which affects the lift due to the inertial reaction.

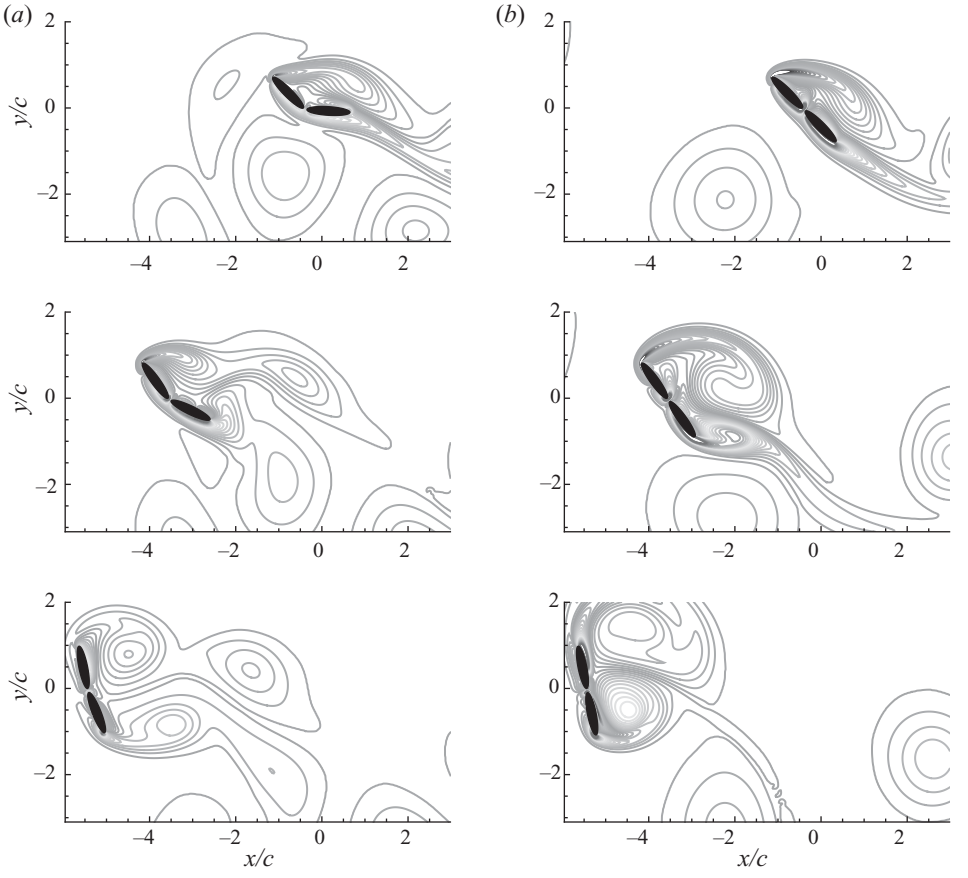

FIGURE 19. Vorticity snapshots for the kinematics $A_0/L = 5.33$, $\Phi = 0$, $X_D/L = 0.48$ for $K = 5.1$ (*a*) and rigidly linked wing (*b*). Rows are at $t/T = 2.51$, 2.61, 2.71, respectively.

Thus, the coupled elastic deflection/vortex shedding mechanism plays an important role in limiting the aerodynamic effectiveness of the wing at relatively high heave amplitudes compared to a corresponding rigid wing.

5.2. *Rigid versus flexible wings at large pitching phase lead*

The last example exhibited a feature of hovering with a flexible wing that generally detracted from the wing's aerodynamic performance. The present example, in contrast, explores a case in which the flexibility of the wing provides aerodynamic benefit. It was found in § 4.3 that the lift generated by flexible wings was much less sensitive than that of a rigid wing to the phase lead of pitching to heaving. This aspect is examined here by comparing a wing with stiffness $K = 23.5$ and a rigid wing, with $A_0/L = 2.67$, $\Phi = 67.5^\circ$ and $X_D/L = 0.48$. Figures 13 and 15 show that, for this case, the mean lift of the flexible wing is more than twice and the efficiency nearly three times that of the rigid wing. The lift and deflection histories of these two wings are depicted in figure 20. The flexible wing maintains a nearly constant backward deflection of approximately 25° in each heaving half-stroke. At early times, the lift generated by the two wings is nearly identical. However, the lift of the rigid wing changes dramatically after approximately two full strokes, with large negative excursions between the peaks, while the lift of the flexible wing remains principally unchanged.

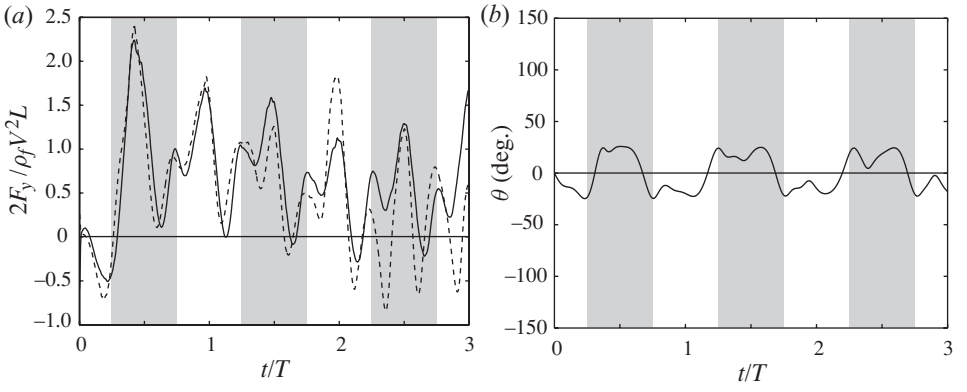

FIGURE 20. Lift (a) and hinge deflection (b) histories for $A_0/L = 2.67$, $\Phi = 67.5^\circ$ and $X_D/L = 0.48$. —, $K = 23.5$ and – –, rigidly linked bodies.

The vorticity generated by these wings during a wing-reversal event is depicted in figure 21. The most notable difference in the flows produced by the wings lies in the behaviour of the leading-edge vortex. In the flexible wing, the leading-edge vortex generated in the previous half-stroke is re-encountered during the rotation in the depicted sequence. The vortex travels downwards towards the trailing edge, where it is accommodated into the wake by the deflecting passive section as the wing initiates its heave in the positive x direction. Furthermore, the counterclockwise vortex generated at the trailing edge at $t/T = 2.71$ as the passive section is deflected pairs with the starting vortex of opposite sign generated by the subsequent heave. This pair propagates in the $-x$ direction, which clears it from the vicinity of the flapping wing. Consequently, the wing encounters a basically quiescent flow during the ensuing half-stroke, allowing it to cleanly generate a new leading-edge vortex and the associated lift.

In contrast, the re-encountered leading-edge vortex lingers much longer in front of the rigid wing. The most negative lift occurs at approximately $t/T = 2.91$, when this vortex sits directly in front of and below the wing and applies a significant downwards suction. Furthermore, there is no counterclockwise vortex to pair with the starting vortex developed at the trailing edge at $t/T = 2.81$, so this vorticity tends to remain in the vicinity of the wing. The persistence of previously shed vorticity prevents any noticeable leading-edge vortex from developing in the following heave, and the usual lift peak from heave at $t/T \approx 3$ is drastically reduced compared to the previous half-stroke. This behaviour is clearly highly transient, changing significantly from half-stroke to half-stroke due to the nonlinear interaction of the shed vortices.

The tendency for the re-encountered leading-edge vortex to quickly slide into the wake and for trailing-edge vortices to pair and propagate away appear to be crucial for maintaining consistent lift from cycle to cycle. The flexible wing accommodates the sliding vortex by deflecting out of its path. A similar behaviour – not shown – is exhibited by the wings with stiffness $K = 5.1$ and $K = 51.4$.

6. Conclusion

This paper has used high-resolution simulations to examine the effect of flexibility on the aerodynamic performance of a two-dimensional wing in hovering motion. The mean lift, mean power and the lift per unit power have each been computed to

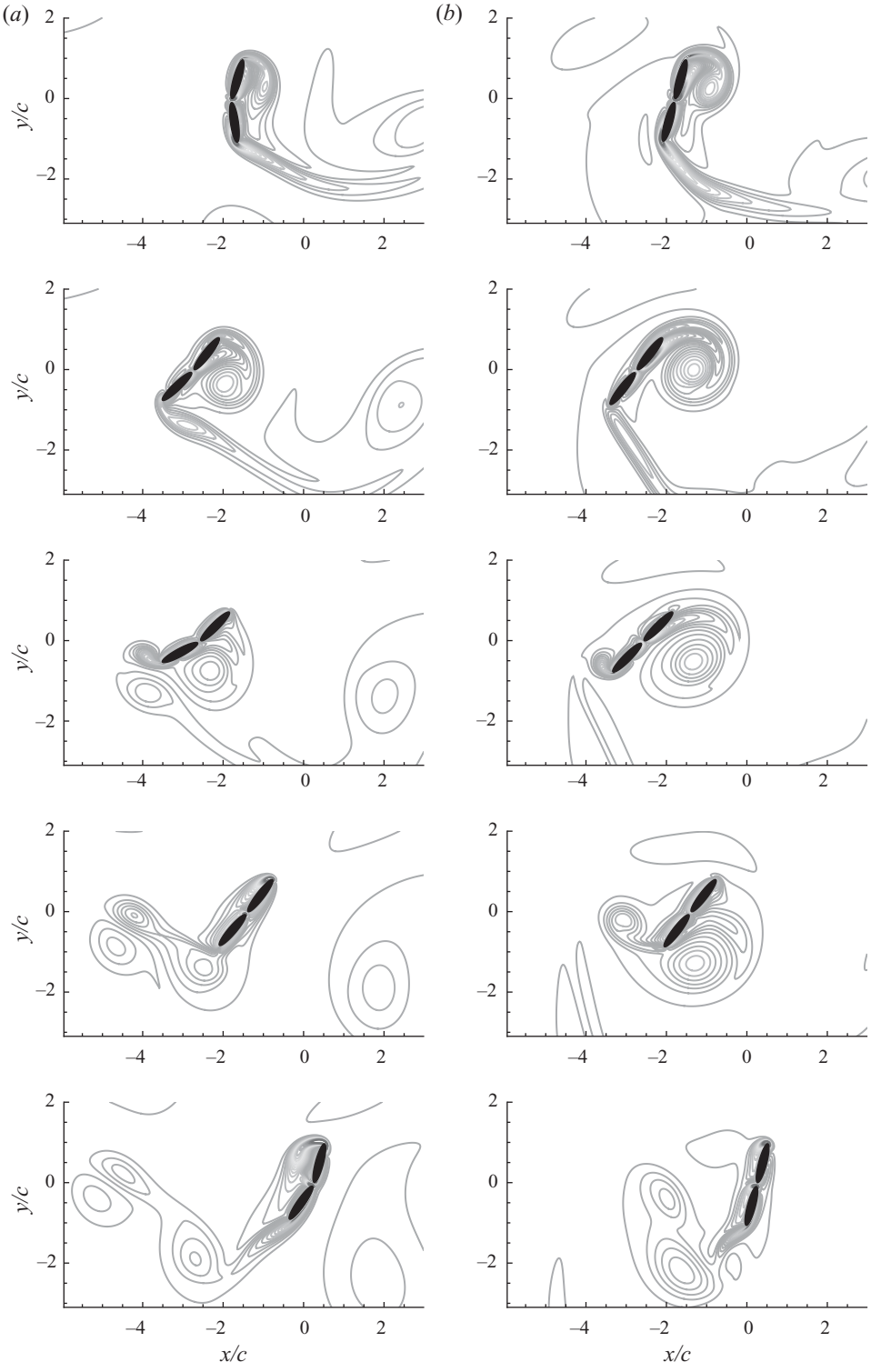

FIGURE 21. Vorticity snapshots for the kinematics $A_0/L = 2.67$, $\Phi = 67.5^\circ$ and $X_D/L = 0.48$ for $K = 23.5$ (*a*) and rigidly linked wing (*b*). Rows are at $t/T = 2.61$, 2.71, 2.81, 2.91, 3.01, respectively.

measure the effectiveness of the flapping wing. It has been shown that wing flexion generally reduces the power consumed by flapping compared to a rigid wing. However, flexion also limits the effectiveness of the wing at relatively large heave amplitudes, as the coupled dynamics of the wing and the leading-edge vortices cause the latter to prematurely detach, thereby truncating the well-known lift enhancement from the leading-edge vortex.

However, wing flexibility provides a notable benefit in reducing the sensitivity of lift generation to the phase lead of pitching to heaving. A flexible wing is more able than a rigid wing to accommodate a shed leading-edge vortex into the wake during wing reversal and to generate counter-rotating pairs of trailing-edge vortices that propagate away, and can thereby clear its path for generating circulatory lift from a new leading-edge vortex on the ensuing heave. Flexibility also provides opportunities for lift generation when the wing remains nearly vertical, as the passive deflection reduces the effective angle of attack. It was shown that the effective pitch angle can be determined from a line connecting the centroids of the first and last bodies.

More work is still needed to elucidate the role of flexibility in hovering-mode flapping. This investigation has primarily focused on identification of important mechanisms through which 'flexibility' – as a generic concept – can significantly alter the aerodynamic performance of a flapping wing in hovering, and has made only a limited attempt to quantify the dependence of these mechanisms on stiffness (e.g. through frequency response). Furthermore, this study has examined only a planar model problem, which is almost certainly inadequate as a surrogate for a full three-dimensional flapping wing. It remains to be seen whether the phenomena observed in this investigation play some analogous role in three-dimensional flapping. For example, the enhanced stability of the leading-edge vortex that has been attributed to the spanwise flow (Maxworthy 1979) will likely be affected by the deflection of the wing, as observed in the two-dimensional examples with large heave amplitude explored in the present paper. It will also be interesting to see if the increased robustness of the lift and efficiency of flexible wings to changes in pitching/heaving phase persists in full flapping. These issues will be explored in future work.

Support for this work by the National Science Foundation, under award CBET-0645228, is gratefully acknowledged.

REFERENCES

van den Berg, C. & Ellington, C. P. 1997 The three-dimensional leading-edge vortex of a 'hovering' model hawkmoth. *Phil. Trans. R. Soc. Lond.* B **352**, 329–340.

Bergou, A. J., Xu, S. & Wang, Z. J. 2007 Passive wing pitch reversal in insect flight. *J. Fluid Mech.* **591**, 321–337.

Brunton, S. L., Rowley, C. W., Taira, K., Colonius, T., Collins, J. & Williams, D. R. 2008 Unsteady aerodynamic forces on small-scale wings: experiments, simulations and models. *AIAA Paper* 2008-0520.

Combes, S. A. & Daniel, T. L. 2003 Into thin air: contributions of aerodynamic and inertial-elastic forces to wing bending in the hawkmoth *Manduca sexta*. *J. Exp. Biol.* **206**, 2999–3006.

Dickinson, M. H., Lehmann, F.-O. & Sane, S. P. 1999 Wing rotation and the aerodynamic basis of insect flight. *Science* **284**, 1954–1960.

Dudley, R. 2000 *The Biomechanics of Insect Flight: Form, Function and Evolution*. Princeton University Press.

Eldredge, J. D. 2007 Numerical simulation of the fluid dynamics of 2D rigid body motion with the vortex particle method. *J. Comput. Phys.* **221**, 626–648.

Eldredge, J. D. 2008 Dynamically coupled fluid–body interactions in vorticity-based numerical simulations. *J. Comput. Phys.* **227**, 9170–9194.

Ellington, C. P. 1984 The aerodynamics of hovering insect flight. 3. Kinematics. *Phil. Trans. R. Soc. Lond.* B **305**, 41–78.

Maxworthy, T. 1979 Experiments on the Weis–Fogh mechanism of lift generation by insects in hovering flight. Part 1. Dynamics of the 'fling'. *J. Fluid Mech.* **93**, 47–63.

Michelin, S., Llewelyn Smith, S. G. & Glover, B. J. 2008 Vortex shedding model of a flapping flag. *J. Fluid Mech.* **617**, 1–10.

Toomey, J. 2009 Numerical and experimental studies of flexibility in flapping wing aerodynamics. PhD thesis, University of California, Los Angeles, CA.

Toomey, J. & Eldredge, J. D. 2008 Numerical and experimental study of the fluid dynamics of a flapping wing with low order flexibility. *Phys. Fluids* **20**, 073603.

Vandenberghe, N., Zhang, J. & Childress, S. 2004 Symmetry breaking leads to forward flapping flight. *J. Fluid Mech.* **506**, 147–155.

Vanella, M., Fitzgerald, T., Preidikman, S., Balaras, E. & Balachandran, B. 2009 Influence of flexibility on the aerodynamic performance of a hovering wing. *J. Exp. Biol.* **212**, 95–105.

Wang, Z. J. 2000 Vortex shedding and frequency selection in flapping flight. *J. Fluid Mech.* **410**, 323–341.

Wang, Z. J. 2005 Dissecting insect flight. *Annu. Rev. Fluid Mech.* **37**, 183–210.

Wang, Z. J., Birch, J. M. & Dickinson, M. H. 2004 Unsteady forces and flows in low Reynolds number hovering flight: two-dimensional computations vs. robotic wing experiments. *J. Exp. Biol.* **207**, 449–460.